Electrochemical Impedance Spectroscopy and First-Principle Investigations on the Oxidation Mechanism of Hypophosphite Anion in the Electroless Deposition System of Nickel

Guofeng Cui,*,† Hong Liu,† Gang Wu,‡ Jianwei Zhao,*,§ Shuqin Song,|| and Pei Kang Shen||

School of Chemistry and Chemical Engineering, Sun Yat-sen University, Guangzhou 510275, China, Department of Chemical Engineering, University of South Carolina, Columbia, South Carolina 29208, Department of Chemistry, Nanjing University, Nanjing 210093, China, and State Key Laboratory of Optoelectronic Materials and Technologies, School of Physics and Engineering, Sun Yat-sen University, Guangzhou 510275, China

Received: October 4, 2007; In Final Form: December 13, 2007

In this work, the oxidation mechanism of hypophosphite anion ($H_2PO_2^-$) in acidic and alkaline media in the presence of Ni(II) specie was investigated by using electrochemical impedance spectroscopy (EIS) and density functional theory (DFT). In EIS, three major electrochemical processes in the electroless deposition process were found, when the solution pH ranged from 5.5 to 9.5. To understand the microscopic mechanisms involved, all participate species in the reaction pathways were calculated by the DFT method along with a natural bond orbital (NBO) analysis. Two emulating reactions were demonstrated: Path (I) passes through a primary dehydrogenation (D-RP), and Path (II) includes a primary addition of OH^- (A-RP) on the hypophosphite anion. By comparison of the energy levels of all species, it can be concluded that Path (II) is energetically favorable under both acidic and alkaline conditions. The DFT and NBO analysis can provide strong evidence for the loops detected in the EIS, especially especially for the inductive loop (IL-M) in the medium-frequency domain that is caused by the formation of $[Ni^I-H_3PO_2(OH)]$ and the capacitive loop (CL-L) in the low-frequency domain by $[H_2PO_2(OH)]$. The combination of electrochemical analysis (EIS) and first principle theory (DFT) analysis proves that it is helpful to explore the nature of the interaction between anodic and cathodic reactions in the electroless deposition process.

1. Introduction

Recently, the synthesis of nanostructured nickel materials, such as core−shell microspheres,[1] nanospheres,[2] hollow microfiber,[3] and microscaled patterned nickel[4,5] has provided the motivation to explore the mechanism of electroless nickel deposition. Although much theoretical and experimental effort has been made in this field, the mechanism is not yet completely understood. Those pioneering works contributed by Homma,[6−8] Touhami[9,10] and Xukuforova[11] are very instructive, indicating that the oxidation of hypophosphite ion is a key step in the whole process.[12]

Electroless nickel deposition is a complicated mixed electrochemical process containing anodic reaction (oxidation of hypophosphite) and cathodic processes (formation of Ni(0), phosphorus atoms, and hydrogen gas).[13,14] The emulating reaction is formed by the three cathodic processes contending for the reducing specie, hydrogen radical in the electroless process. Thus, the emulating reaction is formed on the electrode surface. Those reactions are similar to corrosion to some extent. However, there exist interactions between the anodic and the cathodic processes, and the corresponding involved mechanism is still poorly understood.[15−17] Touhami first used electrochemical impedance spectroscopy (EIS) to investigate these intricate reactions. On the basis of EIS results, he proposed that the interaction may account for special intermediate adsorption of Ni_{ads}^I and $[H_2PO_2(OH)_2]_{ads}^-$.[9,10] Unfortunately, the structure of the possible species causing the EIS special loops could not be determined by using only electrochemical methods.

Theoretical contributions to the oxidation of hypophosphite ion by Homma showed that the primary pathway of the addition of OH^- is energetically favorable in the reaction.[7] However, this pathway model cannot be used to explore the charge-transfer process and the effect of pH value involved in the mechanism.

In our previous experimental works, the electron-transfer process and pH value were found to be two key factors in the process.[18,19] Several experimental observations also remind us that the Ni(II) species may oxidize the hypophosphite anion in bulk solution. For example, in the electroless deposition of nickel, the nanoparticles can be spontaneously generated even in solution, though no substrate is supported.[20−22] Moreover, the redox potential of hypophosphite ion is obviously different in acidic and alkaline solutions, according to the diagram of pH versus potential of the $P-H_2O$ group, as illustrate in eqs 1 and 2.[23]

In acidic solution, we found

$$H_2PO_2^- + H_2O \rightarrow H_2PO_3^- + 2H^+ + 2e^- \qquad E^\theta = -0.504\ \text{V} + 0.06\ \text{pH (V vs. SHE)} \quad (1)$$

* Corresponding authors. E-mail: cuigf@mail.sysu.edu.cn (G. C.), zhaojw@nju.edu.cn (J.Z.). Tel: +86-20-84110560 (G.C.), +86-25-83596523 (J.Z.).

† School of Chemistry and Chemical Engineering, Sun Yat-sen University.

‡ University of South Carolina.

§ Nanjing University.

|| School of Physics and Engineering, Sun Yat-sen University.

10.1021/jp7097119 CCC: $40.75
Published on Web 03/01/2008

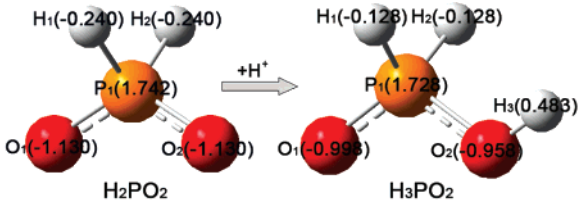

Figure 1. Optimized structure and NBO charge distribution of hypophosphite ion (H_2PO_2) and hypophosphorous acid (H_3PO_2) obtained on the B3LYP/6-311G(d,p) level under the polarizable continuum model (PCM) solvent effect model in water solution.

In alkaline solution, we found

$$H_2PO_2^- + 3OH^- \rightarrow HPO_3^{2-} + 2H_2O + 2e^- \qquad E^\theta = -0.310V + 0.09\ pH\ (V\ vs.\ SHE) \quad (2)$$

Therefore, it is necessary to further understand the effect of pH on the reaction mechanism. This may facilitate precisely controlling the reaction or rationalizing the operation conditions to assist in the exploration of the oxidation mechanism of hypophosphite ion.

In the present work, we tried to combine EIS with density functional theory (DFT) methods to study the oxidation mechanism of hypophosphite ion in acidic and alkaline solutions. The effects of solvent and pH value in the electrolytes also have been explored using an explicit solvation model. The reaction species in possible reaction pathways in acidic and alkaline media are determined by DFT calculations. Moreover, the formation of special loops in EIS is analyzed according to the results of DFT calculations.

2. Experimental Methodology

2.1. Character of pH Values on Electroless Nickel Process by EIS Measurement. EIS measurements were performed in a three-electrode one-compartment cell, in which a 2.0 × 5.0 cm^2 mild carbon steel sheet, a 1.0 × 1.0 cm^2 platinum foil, and a saturated calomel electrode (SCE) were used for the working electrode, the counter electrode, and the reference electrode, respectively. Before the measurement, the working electrode was mechanically polished with 600 and 1200 grade silicon carbide papers. Then it was cleaned with ethanol and acetone. Finally, it was activated in 10.0 mass % H_2SO_4. In the initial stage of EIS measurement, the working electrode was coated by electroless Ni−P alloy. The SCE was protected by a glass tube filled with saturated KCl to prevent pollution of the electrolyte from the SCE.

Electroless nickel solution was prepared with analytical-grade reagents and Millipore ultrapure water. The solutions contained 0.08 M nickel sulfate, 0.21 M sodium hypophosphite, 0.15 M sodium acetate, 0.13 M lactic acid, and 0.06 M propionic acid. Then the pH value of the solution was adjusted by ammonium addition to 5.5, 7.5, and 9.5. In order to avoid man-made interference, the pH was not adjusted again in the whole measurement. The electrolytes were heated to 82 ± 1 °C and purged using nitrogen bubbling before the EIS measurement.

Electrochemical impedance spectra were recorded with a Gamry potentiostat PC4-750 system under the deposition potential. A sinusoidal perturbation of 5 mV was applied at the cell potential over the frequency range of 5 mHz to 100 kHz.

2.2. Character of pH Values on Electroless Nickel Mechanism by DFT Calculations. The calculations were carried out with the *Gaussian 03* program,[24] employing the hybrid Becke exchange and the Lee, Yang, and Parr correlation (B3LYP) functional method.[25−27] In the geometry optimization, single-point energy calculation, transition state location, and Weinhold's natural bond orbital (NBO) analysis 6-311G(d,p) basis set was used for hydrogen, oxygen, and phosphorus atoms, and the LAN2DZ basis set was used for the nickel atom with the Hay and Wadt effective core pseudopotential.[28] These basis sets have also been used by Homma et al.[29] The molecular geometry and vibrational frequency of all species were calculated to determine the mechanism. Stationary points were presumed without any vibration, while transition states were featured with exactly single imaginary vibration.

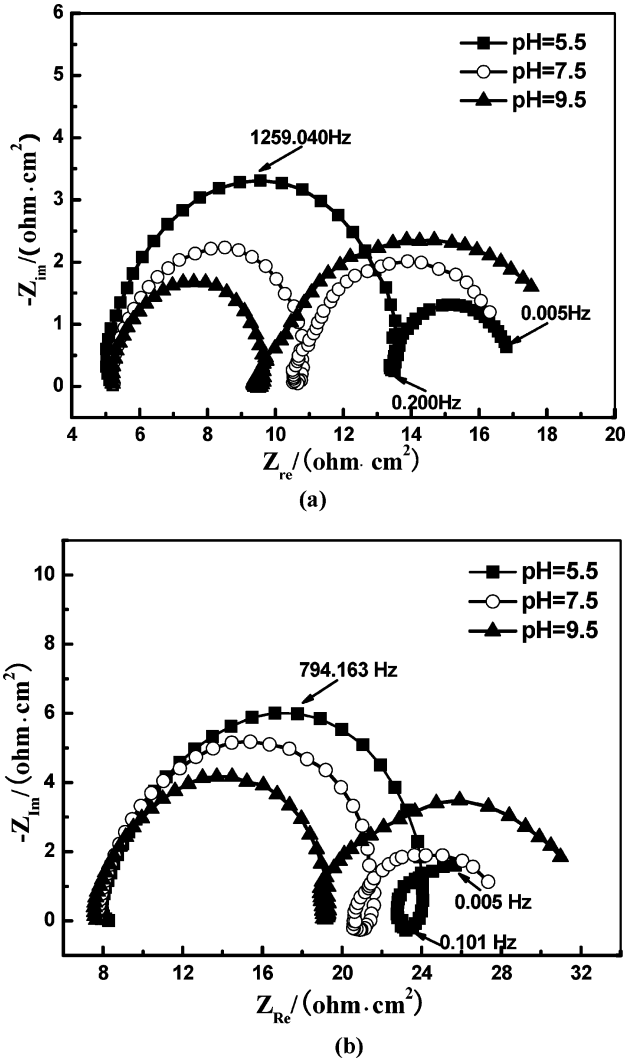

Figure 2. Nyquist impedance spectra for electroless nickel deposition in solutions with pH values of 5.5, 7.5, and 9.5 in the initial immersion (a) and after 1 h immersion time (b) at deposition potential.

Since the oxidation reaction takes place in aqueous solution, a number of factors, especially solvation effect and catalytic activity of the nickel species, may affect the reaction. In the potential energy calculation, solvation effect was considered using an explicit solvation model, in which two water molecules complexing with Ni(II) were used as the reactant. Additionally, metallic catalytic activity was evaluated based on the concentration of Ni(II). Thus, the reaction mechanism can be discussed in a closed system, giving an elaborated electron-transfer route from hyposphosphite ion to Ni(II).

The calculation of hypophosphite ion and hypophosphorous in Section 3.1 were based on the considering water solvation effect as an isodensity surface polarized continuum model

SCHEME 1: Oxidation Mechanism of Hypophosphite Ion in Acidic (a) and Alkaline (b) Solutions

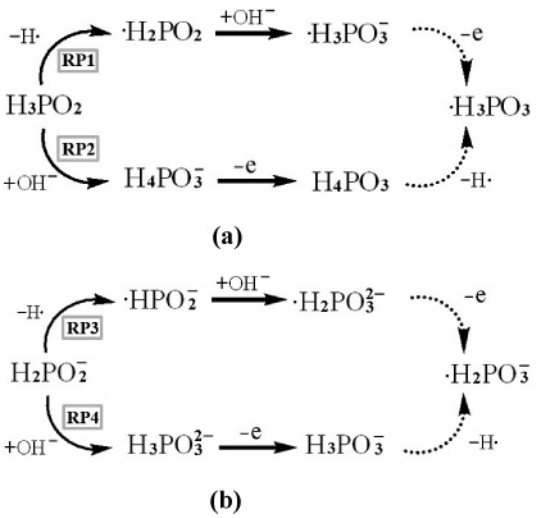

(IPCM).[30−33] In the IPCM calculations, the dielectric constant is set at 60.86 (in the pure water of the bulk solvent)[34] and the temperature is set at 353.15 K.

3. Results and Discussion

3.1. pH Effect of Solution on the Hypophosphite Ion Structure Studied by DFT Calculations. To fully investigate the oxidation mechanism of hypophosphite, it is instructive to discuss the experimental conditions first. As demonstrated in refs 35 and 36, the pH value and temperature of solution are two key factors affecting the reaction rate of electroless nickel deposition. Generally, a high rate or low-temperature electroless deposition of nickel occurs only in alkaline solution. Moreover, the redox potential of hypophosphite ion will shift positively with the increase of pH value, as shown in eqs 1 and 2.

The pH-dependence influence on the oxidation mechanism can be attributed to two effects. One is the different structural feature of the hypophosphite reactant under acidic and alkaline conditions. This will be discussed in detail in this section. The other is that the OH^- or H^+ ions may take part directly in the reaction as a reactant, which will be considered in the following sections.

The optimized geometries and NBO charge distributions were obtained in aqueous solution at 353.15 K as shown in Figure 1. There are two identical P═O bonds and two P−H bonds in the structure of H_2PO_2, in which double $P_1-O_{1(2)}$ and $P_1-H_{1(2)}$ bonds have equal lengths 1.419 and 1.512 Å, respectively. Meanwhile, the bond angles of $H_1-P_1-O_1$, $O_1-P_1-O_2$, and $H_1-P_1-H_2$ are 108.4°, 121.3°, and 99.7° respectively. Additionally, the charge distributions on the $H_{1(2)}$, P_1, and $O_{1(2)}$ atoms are −0.240, 1.742, and −1.130, respectively. Obviously, the hypophosphite ion reveals the C_{2v} symmetric feature. However, the molecular symmetry is destroyed when one proton attacks the oxygen atom (O_2), as illustrated in Figure 1. The bond lengths of P_1-H_1 and P_1-O_1 decrease to 1.401 and 1.486 Å, respectively. At the same time, the bond angles $H_1-P_1-O_1$, $O_1-P_1-O_2$, and $H_1-P_1-H_2$ also change to 114.9°, 112.4°, and 103.9°, respectively. Moreover, the charges on the two oxygen atoms decrease from −1.130 to −0.958 (O_1) and −0.998 (O_2). It should be noticed that the charge on the hydrogen atoms decreases from −0.240 to −0.128, which suggests the protonated structure has a greater capability of hemolytic dissociation of the P_1-H_1 or P_1-H_2 bond.

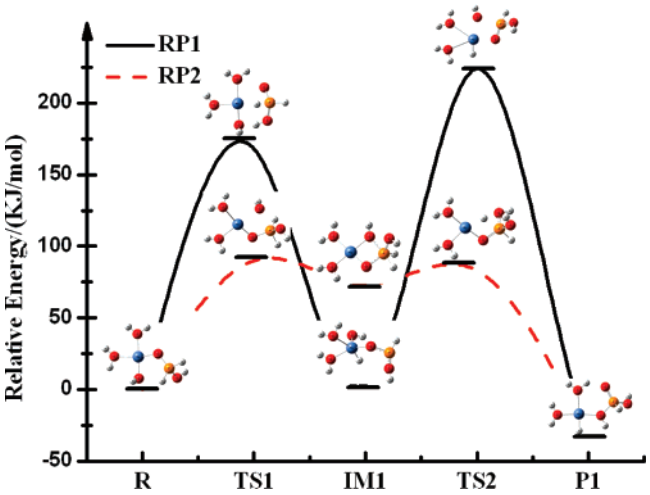

Figure 3. Energy potential profile of the reaction mechanism of hypophosphorous acid oxidized by Ni(II) obtained on the B3LYP/6-311G(d,p) level for main-group atoms and the LANL2DZ level for the nickel atom. Relative energy in kJ/mol (blue spheres represent nickel atoms, yellow spheres represent phosphorus atoms, red spheres represent oxygen atoms, and white spheres represent hydrogen atoms).

3.2. pH Effect on the Electroless Nickel Process Studied by EIS Measurements. There are three characteristic loops on the impedance plots of electroless nickel deposition for the samples immersed into electrolyte at initial time and 1 h later, as illustrated in Figure 2. They are a capacitive loop (CL-H) in the high-frequency domain, an inductive loop (IL-M) in the medium-frequency domain, and a capacitive loop (CL-L) in the low-frequency domain.

For CL-H, it is generally correlated to the discharging and charging process of electrical double layers at the interface of electrode/solution. The loop diameter is determined by the charge-transfer resistance, R_{ct}. During the first hour of reaction, the CL-Hs show significant difference, as shown in Figure 2a, which means the R_{ct} gradually decreases from 8.3 to 5.6 and then to 4.3 ohm·cm^2 with the pH value increasing. The similar case also appears in the second hour, as illustrated in Figure 2b. This case can be attributed to the accelerated electroless deposition rate as the pH value of the solution increases. The experimental results show good agreement with eqs 1 and 2.

The IL-M and CL-L loops are characteristic loops for electroless nickel deposition, which are distinct from corrosion. Moreover, they can provide some strong evidence for the interaction between cathode and anode.

There are three smaller inductive loops in Figure 2 in the medium-frequency domain. It can be attributed to the presence of some unstable surface intermediates.[37] The special intermediate can easily obtain and lose electron(s) from/to another more stable intermediate. In our present system, the process can be generally explained as the process of electron transfer from Ni(I) to Ni(II) and Ni(I) to Ni(0). Touhami et al. proposed that the unstable intermediate is Ni_{ads}^{I}. We will discuss the reason for the formation of IL-M according to the DFT analysis in Section 3.4. There is no significant difference in Figure 2a, and the diameter of IL-M is rather small, probably due to the initial reaction rate being rather rapid. On the other hand, the difference of diameters is quite significant in Figure 2b after 1 h of reaction. It can be explained by the decline of the reaction rate, due to the insufficient supply of reactant and adjustment of pH value during the measurement. Moreover, the diameter of IL-M

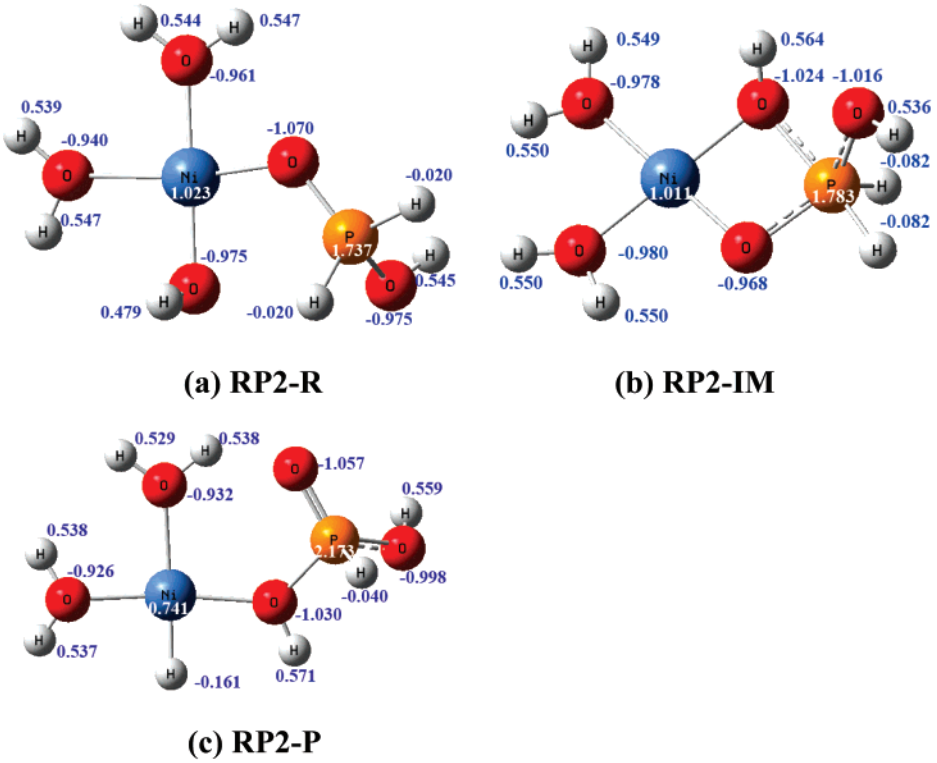

Figure 4. NBO charge distribution of stable reaction species in the oxidation reaction pathway, RP2 of hypophosphorous acid: (a) R1, (b) IM1, and (c) P1.

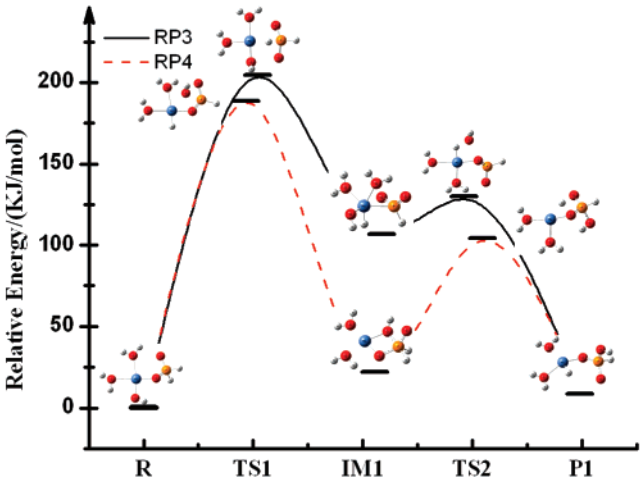

Figure 5. Energy potential profile of the oxidation reaction mechanism of hypophosphite ion oxidized by Ni(II) obtained on the B3LYP/6-311G(d,p) level for main-group atoms and the LANL2DZ level for nickel atom. Relative energy in kJ/mol (blue spheres represent nickel atoms, yellow spheres represent phosphorus atoms, red spheres represent oxygen atoms, white spheres represent hydrogen atoms).

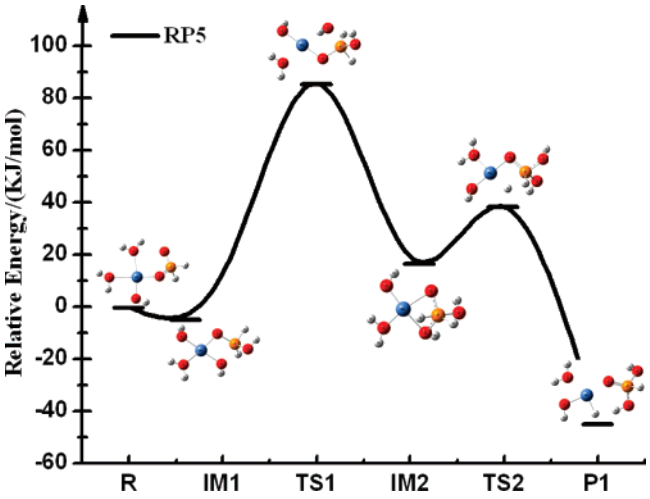

Figure 6. Energy potential profile of the oxidation reaction mechanism of hypophosphite ion oxidized by Ni(II) in RP5 obtained on the B3LYP/6-311G(d,p) level for main-group atoms and the LANL2DZ level for nickel atom. Relative energy is given in kJ/mol (blue spheres represent nickel atoms, yellow spheres represent phosphorus atoms, red spheres represent oxygen atoms, and white spheres represent hydrogen atoms).

gradually decreases with increasing pH value, which can be attributed to the accelerated formation of Ni(I) by the addition of OH^-.

In the low-frequency domain, other capacity loops were observed, as shown in Figure 2. The loops size increases with increasing pH value, which is directly related to the OH^- concentration. One proposition is that the formation of a hydroxyl species on the electrode surface hinders the reaction. Touhami considered that the oxidation of hypophosphite is accompanied by the formation of hydroxyl compounds, $[H_2PO_2(OH)_2]_{ads}^-$, which would partially inhibit the reaction. We will discuss the formation reason of CL-L in Section 3.5 in detail, combining the DFT analysis results.

Comparing parts a and b of Figure 2, three characteristic loops show obvious increments to a different extent. This revealed that the reaction rate decrease gradually in the whole measuring process. The phenomenon can be explained by the exhausted reactant.

3.3. Oxidation Mechanism of Hypophosphite Ion in Acidic and Alkaline Conditions. In general, the oxidation of hypophosphite passes through two possible pathways, as suggested by Homma.[6,7] The first pathway (D-RP) can pass through a direct breakage of the P−H bond and form a hydrogen radical, via RP1 and RP3. The other pathway (A-RP) includes a direct addition of OH^- ion to the phosphorus atom, then one hydrogen radical separates from the phosphorus atom, via RP2 and RP4.

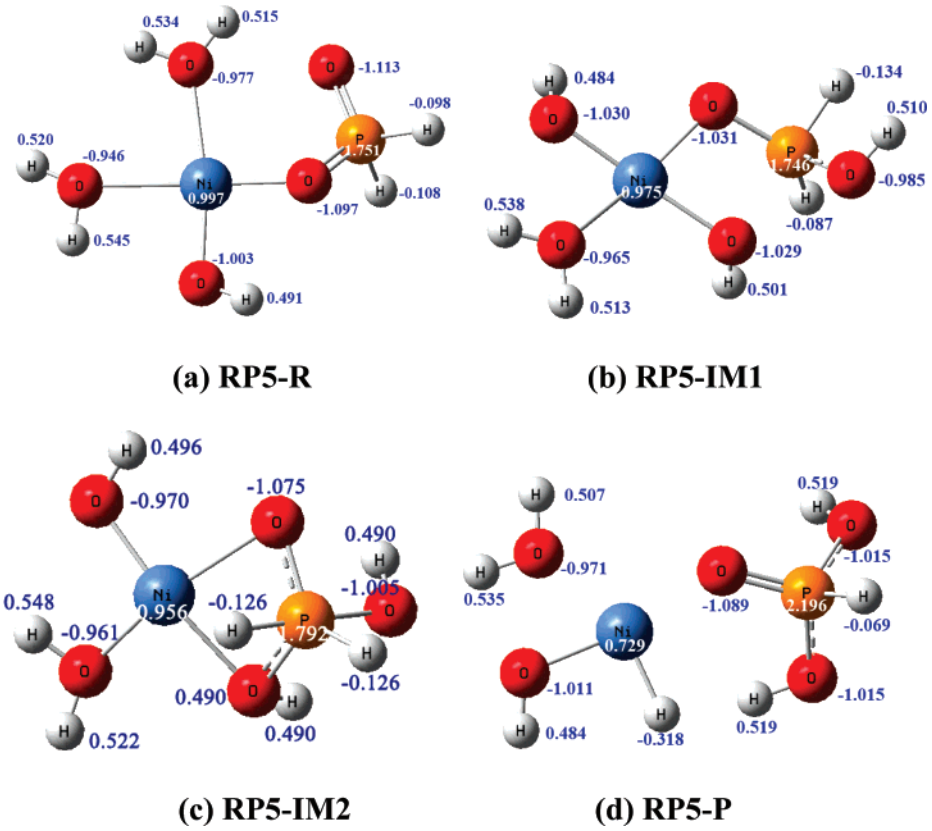

Figure 7. NBO charge distribution of the stable reaction species in the oxidation reaction pathway, RP5 of hypophosphite ion: (a) R1, (b) IM1, (c) IM2, and (d) P1.

Then the hydrogen radical can attack the Ni(II) species and reduce it to Ni(I), even to Ni(0). The proposed reaction pathways, from RP1 to RP4, are described in Scheme 1. In an early theoretical work, Homma had performed theoretical calculation focusing on both RP3 and RP4 and pointed out that RP4 is favorable for the electroless nickel process.[7]

3.4. Oxidation Mechanism of Hypophosphorous Acid in Acidic Solution. Figure 3 shows the optimized geometries of the intermediates and the energy profiles for the oxidation process of $[NiH_3PO_2(H_2O)_2OH]^-$ specie in acidic solution. In this section, we will discuss the reaction pathway of hypophosphorous acid under a simple solvation model, corresponding to RP1 and RP2.

As shown in Figure 3, there are two transition states and one intermediate in the reactions of both RP1 and RP2. On the RP1 profile, the maximum barrier is found to correspond to TS2, which is 224.1 kJ/mol higher than the energy level of IM1. On the other hand, the maximum barrier in route RP2 corresponds to TS1 with 91.0 kJ/mol relative energy. To determine the energetically favorable route, it is instructive to compare the energy levels of the corresponding species in RP1 and RP2. In particular, TS1 has a much relatively higher energy in RP1 than that in RP2. The difference is caused by the charge distribution on the phosphorus atom as inferred by the NBO analysis. TS1 is the addition of OH^- on phosphorus followed by the loss of hydrogen radical. As illustrated in Figure 1, for hypophosphorus acid, the charge on the phosphorus atom is 1.728. Therefore the addition of OH^- becomes easy due to electrostatic interaction.

Obviously, the RP2 path is preferred route for the hypophosphorous oxidation in the acidic solution, based on the relative energy levels. This result is similar to the oxidation of hypophosphorous that occurs on a palladium cluster as calculated by Homma, except for the absolute value of the energy barrier.[7] In their work, the barrier height was estimated to be 254.98 kJ/mol, which is far higher than the result presented in our work. The difference is most likely caused by the catalytic effect of the Ni(II) complex, which is due to the fact that Ni(II) can directly attract the oxygen atom in the hydroxyl ion. This character is especially obvious when the hydroxyl ion attacks phosphorus atom in hypophosphite anion. The special structure may make the formation of the IM1 specie easier and smoother.

The detailed analysis of how electrons transfer from the electron donor is very important in clarifying the oxidation mechanism. The NBO analysis method is powerful and widely employed to determine the donor−acceptor charge transfer in the oxidation reaction process.[38−40] Furthermore, we analyzed the charge distribution of the stable reaction species for RP2 in the closed system. DFT calculation shows significant charge redistribution, when the nickel atom complexes with OH^- and $[H_3PO_2]^-$, as illustrated in Figure 4. The charge on Ni(II) is close to 1.0, far from the initial value (2.0). Additionally, the total charge values of OH^- and $[H_3PO_2]^-$ complexing with Ni(II) are −0.496 and 0.197 in RP2-R1, respectively, which are higher than the initial values of −1.0 and 0.0. With the reaction processing, the total charges of $[H_3PO_4]^-$ and $[H_3PO_3]^-$ are −0.369 and 0.178 in RP2-IM1 and RP2-P, respectively, differing from the initial value of −1.0. Obviously, it was generally explained by the ligands occupied molecular orbital overlapping with the unoccupied nickel metal orbital.[41] It was also explained by the electrostatic interaction of the ionic charge.[42] In this reaction, the Ni(II) specie can attract one electron from ligands and form the $[Ni^I{-}H_3PO_2(OH)]$ compound.

The formation of IL-M can be explained by the generation of the $[Ni^I{-}H_3PO_2(OH)]$ compound according to DFT calcula-

tion results. The Ni(II) ions can obtain one electron and be reduced to Ni(I). At the same time, they can also reverse to Ni(II) ions, while the complex breaks. Moreover, the Ni(I) compound can further be reduced to Ni(0), through obtaining one electron from hydrogen radical, as illustrated in Figure 4c. For the Ni−H group in the RP2-P specie, the hydrogen radical is rather unstable in aqueous solution, which is prone to proton transfer. Furthermore, the [$Ni^{I}-H_3PO_2(OH)$] compound is more unstable than RP2-R and RP2-P, as shown in Figure 3, which can easily pass through the TS1 and TS2 states and transfer to more stable species, RP2-R and RP2-P.

It is worth noting that the NBO total charge of phosphorus and hydrogen atoms in reaction species should be considered. In the reaction process, from RP2-R to RP2-IM1 then to RP2-P, the charges of the phosphorus atom are 1.737, 1.783, and 2.173, which are different from the initial values of 1.0, 1.0, and 2.0, as illustrated in Figure 4. Obviously, the phosphorus atom is a major electron density donator in the whole reaction. Additionally, the NBOs of hydrogen atoms directly combining to the phosphorus atom are −0.020(RP2-R), 0.082(RP2-IM), and −0.040(RP2-P), respectively. The phosphorus atom can also provide some electrons to hydrogen, which gives the possibility for a homolytic reaction between the P−H bond.

3.5. Oxidation Mechanism of Hypophosphite Ion in Alkaline Solution. Figure 5 shows the potential energy surface for the oxidation of hypophosphite ion reacting with Ni(II) ion in alkaline solution. The highest energy barriers from R to TS1 in RP3 and RP4 are 202.6 and 186.2 kJ/mol in the process, respectively. The subsequent reaction can occur spontaneously, after crossing over the highest barrier of TS1. However, in the case of RP2, the two energy barriers are too high to pass through.

RP5 is illustrated in Figure 6 based on the possible reaction pathways. The reactant first transfers to IM1 when it obtains one proton from water. The structure of IM1 is similar to that of RP2-R, except that H_2O is replaced by OH^-. The highest energy barrier is 81.6 kJ/mol in RP5 for the TS1 specie, which is significantly lower than that in RP2. Therefore, this is the most favorable reaction pathway for the oxidation of hypophosphite ion in alkaline solution.

When the favorable reaction pathways of RP2 and RP5 in acidic and alkaline solution are compared, the energy barrier of RP2 is 9.4 kJ/mol higher than that in RP5, indicating that the alkaline environment facilitates electroless nickel deposition at low temperature. The result agrees well with the EIS measurement results, which indicate that the diameters of CL-Hs gradually decrease with an increase of pH values, as shown in Figure 2.

The NBO charge distribution provides a quantitative evaluation of the donor−acceptor delocalization of the reaction. Figure 7 shows the NBO charge distribution of RP5. The reaction pathway of RP5 is similar to that of RP2. The charge for Ni(II) (0.997) is much smaller than the initial value (2.0). Obviously, Ni(II) obtains one electron from ligands and then forms Ni(I), as discussed in Section 3.4. The final product of nickel specie is Ni(I)−H(0), which can self-exchange electrons, consequently producing Ni(0)−H(+).

After analyis of the reaction pathways of the oxidation mechanism of hypophosphite ion in acidic and alkaline solution, it can be observed that A-RP is suitable for the reaction process. The products of RP2 and RP5 contain hypophosphite hydroxyl compound, which is [$H_2PO_2(OH)$]• for both. These products can provide evidence for the formation of a capacitive loop at the low-frequency domain in EIS. We considered [$H_2PO_2(OH)$]• as the key specie adsorbed on the electrode surface and that it inhibited the reaction process. Furthermore, its concentration will increase with OH^- concentration.

4. Conclusions

We have investigated the oxidation mechanism of the hypophosphite ion by reacting it with Ni(II) in acidic and alkaline solutions for the electroless deposition process, using EIS measurement and DFT calculation. There are three characteristic loops assigned to a capacitive loop (CL-H) in the high-frequency domain, an inductive loop (IL-M) in the medium-frequency domain, and a capacitive loop (CL-L) in the low-frequency domain in the EIS. To explore the oxidation mechanism of hypophosphite ions, two possible pathways have been deduced by DFT methods: one is formed via primary dehydrogenation and the other is formed via primary addition of OH^-. On the basis of the relative energy levels of all species, it can be concluded that the latter path is an energetically favored one under acidic and alkaline conditions. According to the results obtained by both methods, the formation of IL-M can be attributed to the formation and breakage of [$Ni^{I}-H_3PO_2(OH)$]. Moreover, the appearance of CL-L is due to the formation of [$H_2PO_2(OH)$]• on the electrode surface.

Acknowledgment. The authors gratefully acknowledge the financial support of the Scientific Research Foundation for Young Teachers of the Sun Yat-Sen University (2006-31000-1131214). We also thank Drs. Mingbo Zhang and Jie Zhao for helpful discussions.

References and Notes

(1) Tierno, P.; Goedel, W. A. *J. Phys. Chem. B* **2006**, *110*, 3043.
(2) Xie, S.; Qiao, M.; Zhou, W.; Luo, G.; He, H.; Fan, K.; Zhao, T.; Yuan, W. *J. Phys. Chem. B* **2005**, *109*, 24361.
(3) Ishii, D.; Nagashima, T.; Udatsu, M.; Sun, R. D.; Ishikawa, Y.; Kawasaki, S.; Yamada, M.; Iyoda, T.; Nakagawa, M. *Chem. Mater.* **2006**, *18*, 2152.
(4) Hendricks, T. R.; Dams, E. E.; Wensing, S. T.; Lee, I. *Langmuir* **2007**, *23*, 7404.
(5) Nakagawa, M.; Nawa, N.; Iyoda, T. *Langmuir* **2004**, *20*, 9844.
(6) Homma, T.; Komatsu, I.; Tamaki, A.; Nakai, H.; Osaka, T. *Electrochim. Acta* **2001**, *47*, 47.
(7) Nakai, H.; Homma, T.; Komatsu, I.; Osaka, T. *J. Phys. Chem. B* **2001**, *105*, 1701.
(8) Homma, T.; Tamaki, A.; Nakai, H.; Osaka, T. *J. Electroanal. Chem.* **2003**, *559*, 131.
(9) Touhami, M. E.; Chassaing, E.; Cherkaoui, M. *Electrochim. Acta* **1998**, *43*, 1721.
(10) Touhami, M. E.; Chassaing, E.; Cherkaoui, M. *Electrochim. Acta* **2003**, *48*, 3651.
(11) Xukuforova, A. A.; Kabakov, G. A. *Electrochemistry* **1967**, *3*, 1207.
(12) Han, K. P.; Fang, J. L. *J. Appl. Electrochem.* **1996**, *26*, 1273.
(13) Jusys, Z.; Liaukonis, J.; Vaskelis, A. *J. Electroanal. Chem.* **1992**, *325*, 247.
(14) Kim, Y. S.; Sohn, H. J. *J. Electrochem. Soc.* **1996**, *143*, 505.
(15) Van der Meeraker, J. W. *J. Appl. Electrochem.* **1981**, *11*, 395.
(16) Gafin, A. H.; Orchard, S. W. *J. Appl. Electrochem.* **1992**, *22*, 830.
(17) Gafin, A. H.; Orchard, S. W. *J. Electrochem. Soc.* **1993**, *140*, 3458.
(18) Guofeng, C.; Ning, L.; Deyu, L.; Minglei, C. *J. Electrochem. Soc.* **2005,** 152, C669**.**
(19) Guofeng, C.; Ning, L.; JianWei, Z.; Mingbo, Z. *J. Electrochem. Soc.* **2005,** 152, C861**.**
(20) Yin, X.; Hong, L.; Chen, B. H. *J. Phys. Chem. B* **2004**, *108*, 10919.
(21) Yin, X.; Hong, L.; Chen, B.-H.; Ko, T.-M. *J. Colloid. Interface Sci.* **2003**, *262*, 89.
(22) Chen, C. H.; Chen, B. H.; Hong, L. *Chem. Mater.* **2006**, *18*, 2959.
(23) Lin, S. C.; Chen, S. Y.; Cheng, S. Y.; Lin, J. C. *Solid State Sci.* **2005**, *7*, 897.
(24) Frisch, M. J.; Trucks, G. W.; Schlegel, H. B.; Scuseria, G. E.; Robb, M. A.; Cheeseman, J. R.; Montgomery, J. A., Jr.; Vreven, T.; Kudin, K. N.; Burant, J. C.; Millam, J. M.; Iyengar, S. S.; Tomasi, J.; Barone, V.; Mennucci, B.; Cossi, M.; Scalmani, G.; Rega, N.; Petersson, G. A.;

Nakatsuji, H.; Hada, M.; Ehara, M.; Toyota, K.; Fukuda, R.; Hasegawa, J.; Ishida, M.; Nakajima, T.; Honda, Y.; Kitao, O.; Nakai, H.; Klene, M.; Li, X.; Knox, J. E.; Hratchian, H. P.; Cross, J. B.; Adamo, C.; Jaramillo, J.; Gomperts, R.; Stratmann, R. E.; Yazyev, O.; Austin, A. J.; Cammi, R.; Pomelli, C.; Ochterski, J. W.; Ayala, P. Y.; Morokuma, K.; Voth, G. A.; Salvador, P.; Dannenberg, J. J.; Zakrzewski, V. G.; Dapprich, S.; Daniels, A. D.; Strain, M. C.; Farkas, O.; Malick, D. K.; Rabuck, A. D.; Raghavachari, K.; Foresman, J. B.; Ortiz, J. V.; Cui, Q.; Baboul, A. G.; Clifford, S.; Cioslowski, J.; Stefanov, B. B.; Liu, G.; Liashenko, A.; Piskorz, P.; Komaromi, I.; Martin, R. L.; Fox, D. J.; Keith, T.; Al-Laham, M. A.; Peng, C. Y.; Nanayakkara, A.; Challacombe, M.; Gill, P. M. W.; Johnson, B.; Chen, W.; Wong, M. W.; Gonzalez, C.; Pople, J. A. *Gaussian 03*, revision C.02; Gaussian Inc.: Pittsburgh, PA, 2003.

(25) Kohn, W.; Becke, A. D.; Parr, R. G. *J. Phys. Chem.* **1996**, *100*, 12974.

(26) Becke, A. D. *J. Chem. Phys.* **1993**, *98*, 5648.

(27) Lee, C.; Yang, W.; Parr, R. D. *Phys. Rev. B: Condens. Matter Mater. Phys.* **1988**, *37*, 785.

(28) Hay, P. J.; Wadt, W. R. *J. Chem. Phys.* **1985**, *82*, 301.

(29) Shimada, T.; Sakata, K.; Homma, T.; Nakai, H.; Osaka, T. *Electrochim. Acta* **2005**, *51*, 906.

(30) Miertus, S.; Scrocco, E.; Tomasi, J. *Chem. Phys.* **1981**, *55*, 117.

(31) Barone, V.; Cossi, M.; Mennucci, B.; Tomasi, J. *J. Chem. Phys.* **1997**, *107*, 3210.

(32) Cossi, M.; Barone, V.; Mennucci, B.; Tomasi, J. *Chem. Phys. Lett.* **1998**, *286*, 253.

(33) Barone, V.; Cossi, M.; Tomasi, J. *J. Comput. Chem.* **1998**, *19*, 404.

(34) Dean, J. A. *Lange's Handbook of Chemistry*, 15th ed.; McGraw-Hill Book Co.: New York, 1999; Chapter 5, p 5.134.

(35) Magagnin, L.; Sirtori, V.; Seregni, S.; Origo, A.; Cavallotti, P. L. *Electrochim. Acta* **2005**, *50*, 4622.

(36) Gylienė; O.; Vaškelis, A.; Tarozaitė; R.; Jagminienė; A. *Chemija* **2007**, *18*, 2.

(37) Cao, C. N.; Zhang, J. Q. *An Introduction to Electrochemical Impedance Spectroscopy*; Science Press: Beijing, 2002; Chapter 4, p 78.

(38) Kaneno, D.; Tomoda, S. *Org. Lett.* **2003**, *5*, 2947.

(39) Alabugin, I. V.; Manoharan, M.; Weinhold, F. A. *J. Phys. Chem. A* **2004**, *108*, 4720.

(40) Tormena, C. F.; Dias, L. C.; Rittner, R. *J. Phys. Chem. A* **2005**, *109*, 6077.

(41) Ortega, D. T.; Pandiyan, T.; Cruz, J.; Ochoa, E. G. *J. Phys. Chem. C* **2007**, *111*, 9853.

(42) Costa, D.; Martra, G.; Che, M.; Manceron, L.; Kermarec, M. *J. Am. Chem. Soc.* **2002**, *124*, 7210.